A practical method for calculating thermally-induced stresses in pile foundations used as heat exchangers

Ryan Yin Wai Liu, MEng ACGI AFHEA, Postgraduate Researcher

Eleonora Sailer, MEng MSc DIC, Postgraduate Researcher

David M.G. Taborda, MEng PhD DIC, Senior Lecturer

David M. Potts, BSc PhD DSc FREng FICE FCGI, GCG Professor of Geotechnical Engineering

Lidija Zdravković, MEng MSc PhD DIC, Professor of Computational Geomechanics

Department of Civil and Environmental Engineering, Imperial College London, UK

Corresponding author:

Ryan Yin Wai Liu

Skempton Building, Imperial College London, South Kensington Campus, London, SW7 2AZ

+44 (0)20 7594 6077

ryan.liu13@imperial.ac.uk

ABSTRACT

Thermo-active piles are capable of providing both structural stability as foundations and low carbon heating and cooling as ground source heat exchangers. When subjected to heating or cooling, the soil surrounding the pile restricts its expansion or contraction, giving rise to thermally-induced axial stresses, which need to be considered during design. Previous numerical studies often assume axisymmetry of the problem and/or a simplification of the heating or cooling mechanism of the pile. To simulate accurately the development of thermally-induced axial stresses, this paper presents a computational study comprising three-dimensional fully coupled thermo-hydro-mechanical finite element analyses conducted using the Imperial College Finite Element Program (ICFEP), where the heating of a thermo-active pile is simulated by prescribing a flow of hot water through the heat exchanger pipes within the pile. The effects of pipe arrangement on thermally-induced axial stresses are investigated by considering three different cases – single U-loop, double U-loop and triple U-loop. Since three-dimensional analyses are computationally expensive, a simplified method using a combination of two-dimensional analyses is proposed to estimate the thermally-induced axial stresses, which is subsequently validated and shown to yield accurate results.

NOTATION

a, b, r, s	stiffness degradation parameters
C_p	specific heat capacity
C_w	specific heat capacity of water
c'	cohesion
E	Young's modulus
E_d	deviatoric strain
G_{ref}	maximum shear modulus at reference mean effective stress
G_{tan}	tangent shear modulus
K_f	bulk modulus of pore fluid
K_{ref}	maximum bulk modulus at reference mean effective stress
K_{tan}	tangent bulk modulus
K_0	coefficient of earth pressure
k	permeability
k_0, B	non-linear permeability model parameters
L	pile length
m_G, m_K	parameters defining the dependence of elastic stiffness on mean effective stress
$n_{U-loops}$	number of U-loops
p'	mean effective stress
p'_{ref}	reference mean effective stress
Q	water flow rate
$R_{G,min}$	minimum normalised value of G_{tan}
$R_{K,min}$	minimum normalised value of K_{tan}
r_{pipes}	the radial distance at which the pipes are located within the thermo-active pile
S_u	undrained shear strength
T	temperature
T_{in}	temperature of water entering the thermo-active pile
$T_{in,mid}$	temperature of water in the pipe going down the pile at pile mid-depth
T_{out}	temperature of water leaving the thermo-active pile

$T_{out,mid}$	temperature of water in the pipe going up the pile at pile mid-depth
T_{tbc}	the temperature that is prescribed as a thermal boundary condition in the axisymmetric coupled THM analysis
t	time
α	adhesion factor
α_f	linear coefficient of thermal expansion of pore fluid
α_s	linear coefficient of thermal expansion of soil skeleton
γ_s	specific weight
ΔE	heat flux of thermo-active pile
ΔT	change in temperature
ε_{vol}	volumetric strain
λ	thermal conductivity
μ	Poisson's ratio
ρ	density
ρ_w	density of water
σ_T	thermally-induced axial stress
$\overline{\sigma_T}$	cross-sectionally averaged thermally-induced axial stress
$\overline{\sigma_T}_{max}$	maximum cross-sectionally averaged thermally-induced axial stress over the pile length
ϕ'	angle of shearing resistance
ψ'	angle of dilation

1 INTRODUCTION

The growing demand for renewable energy in recent years has promoted the use of thermo-active piles as a foundation strategy. In particular, stricter sustainability targets requiring that an increasing proportion of energy demand is met by on-site renewable sources (e.g. Merton Rule (Merton Council, 2010; World Wide Fund For Nature, 2019)), have further encouraged the use of thermo-active piles over other renewable energy production methods, especially in dense urban settings.

In addition to guaranteeing structural stability, thermo-active piles can also provide low carbon heating and cooling by exchanging heat with the ground. This is accomplished by circulating a cold or hot fluid through heat exchanger pipes, which are often attached to the reinforcement cage of the pile, extracting or storing heat from/into the ground. The heated or cooled fluid can then be used for heating or cooling above ground structures via a heat pump. As a consequence of the heat exchange, the temperature of the pile increases or reduces, which leads to thermal expansion or contraction, respectively. This deformation is restricted by the surrounding soil, hence inducing axial stresses within the pile, as observed in Laloui et al. (2006) and Bourne-Webb et al. (2009). Given the thermal origin of the deformation and therefore, indirectly, of the mechanical action, these stresses are termed thermally-induced. With time, when a temperature field is slowly developed in the proximity of the thermo-active pile, the soil expands or contracts with the pile, hence reducing the restriction it imposed onto the pile, thereby reducing the thermally-induced axial stresses. This transient effect has been reported in previous numerical studies (Gawecka et al., 2017; Liu et al., 2019) on thermo-active piles. While piles are designed to withstand the stresses due to mechanical loading they are subjected to, when they are used as heat exchangers, thermally-induced stresses need to be accounted for (e.g. in cooling mode, i.e. the pile heating up, there will be an increase in compressive stresses).

The majority of numerical studies reported in the literature (e.g. Laloui et al., 2006; Bodas Freitas et al., 2013; Yavari et al., 2014; Gawecka et al., 2016; Gawecka et al., 2017; Liu, 2017; Anongphouth et al., 2018) on thermo-active piles assume that the problem is axisymmetric, and that the heating or cooling of the pile is simulated by prescribing a simplified thermal boundary condition (such as a uniform change in temperature of the pile, or a uniform volume or line heat flux). Such an approach, while computationally efficient, fails to account for the discrete nature of the heat exchanger pipes used to transfer heat to the pile and the resulting non-uniform temperature field which gives rise to spatial variations of axial stresses. Conversely, in this paper, the explicit modelling of heat exchanger pipes as a form of simulating with greater accuracy the application of thermal loading (similar to other studies, such as Hassani Nezhad Gashti et al. (2014), Batini et al. (2015) and Rotta Loria and Laloui (2016)) is combined with a detailed simulation of the nonlinear coupled thermo-hydro-mechanical (THM) behaviour of soil (as described in Gawecka et al. (2017)) in three-dimensional (3D) finite-element (FE) analyses using the Imperial College Finite Element Program (ICFEP, Potts & Zdravkovic, 1999; Potts & Zdravkovic, 2001; Cui et al., 2018b). In the present analyses, the heating of the thermo-active pile is simulated by prescribing a flow of hot water through pipes embedded within the pile. Different pipe configurations within piles of different diameters are analysed and their effect on the evolution of thermally-induced axial stresses with time is evaluated. These analyses provide more detailed modelling of the heat fluxes taking place within the thermo-active pile compared to analyses where axisymmetry is assumed or simplified thermal boundary conditions are adopted to simulate the heating or cooling of the pile. However, 3D fully coupled THM analyses are computationally expensive, given the large number of degrees of freedom within the numerical model. Hence, after establishing the three-dimensional response of thermo-active piles, a simplified method to estimate the associated thermally-induced axial stresses is proposed. This practical approach involves a combination of two-dimensional (2D) thermal analysis and an axisymmetric coupled THM analysis, leading to a considerable reduction in the computational effort. The performance of the proposed method is verified by comparing the axial stresses obtained in the axisymmetric analyses to those evaluated in the corresponding 3D analyses. It should be noted that, throughout this paper, the sign convention is such that tension is taken as positive.

2 3D THM FE SIMULATION

In order to model the development of thermally-induced axial stresses accurately when a thermo-active pile is subjected to changes in temperature, 3D THM FE analyses are conducted, where the heat injection is simulated by prescribing a flow of hot water through the pipes within the pile. A pile length of $25m$ and two different pile diameters ($600mm$ and $900mm$) are adopted, with three different pipe arrangements (single U-loop – 1U, double U-loop – 2U and triple U-loop – 3U) being considered. Moreover, the pile is assumed to be unrestrained at the surface (i.e. any eventual restraint from the superstructure is disregarded), meaning that it is free to displace vertically during thermal loading. This ensures that any thermally-induced axial stresses are solely due to the restraints applied by the soil, magnifying the importance of the transient response of the pile-soil system, which occupies a central role in this paper. A detailed discussion on the effects of end-restraints and how these affect the response of thermo-active piles can be found in Amatya et al. (2012) and Bourne-Webb et al. (2013). This establishes a set of analyses to enable the verification of the performance of the proposed method to model thermo-active piles in axisymmetric analyses (introduced in Section 3) for different characteristics of thermo-active piles.

2.1 Mesh, stratigraphy and types of elements

The modelled thermo-active pile is assumed to be installed in an idealised deposit consisting solely of London Clay, as adopted in Gawecka et al. (2016). The discretised domain is $64m$ deep and $80m$ in diameter, as illustrated in Figure 1 for the $900mm$ diameter pile (note that only half of the employed mesh is shown for clarity). A detail of the discretisation adopted for the cross-section of the pile is depicted in Figure 2. Moreover, it should be noted that, for the cases with double and triple U-loops, while the geometry of the analysed problem includes at least one plane of symmetry (see e.g. Olgun et al. (2014)), the full section is required since the heat exchange taking place through the heat exchanger pipes at discrete locations within the cross-section of the pile implies non-symmetric temperature fields.

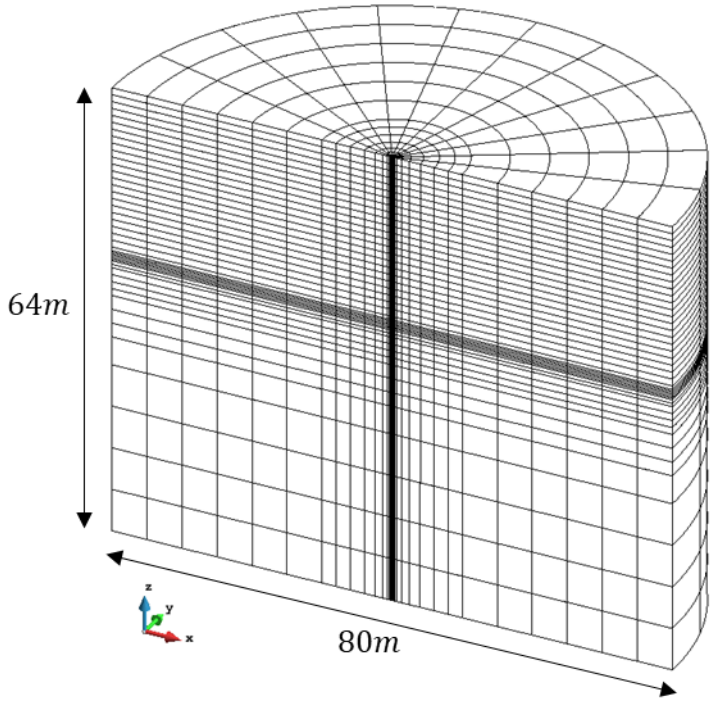

Figure 1 Half of the FE mesh for the analyses on the $900mm$ diameter thermo-active pile

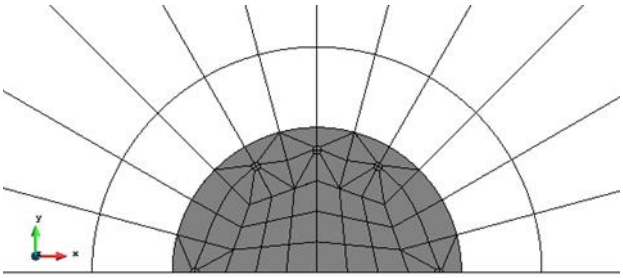

Figure 2 Plan view of half of the zoomed-in FE mesh detailing the pile (shaded in grey)

20-noded isoparametric elements are used to discretise the thermo-active pile and London Clay, with three displacement and one temperature degrees of freedom at each node. For the elements discretising the London Clay, pore water pressure degrees of freedom also exist at their corner nodes. Similar to the modelling procedure adopted in Gawecka et al. (2017) when reproducing the response of the thermo-active test pile at Lambeth College (Bourne-Webb et al., 2009), no interface elements were included in the analyses reported in this study, meaning that any failure

along the pile shaft will be governed by the shear strength of the soil. The pipes within the thermo-active pile that allow water to circulate are discretised with one-dimensional 3-noded bar elements (Gawecka et al., 2018), with three displacement and one temperature degrees of freedom at each node, and pore water pressure degrees of freedom at the end nodes. These pipes are surrounded by a fictitious thermally-enhanced material (TEM), which are modelled using solid elements, characterised by a higher conductivity than that of concrete, to ensure that, in the performed numerical analyses, the correct heat transfer takes place from the pipes to the surrounding medium. The cross-sectional area of the TEM corresponds to that of the inside of the pipe used in the problem being simulated ($5.39 \times 10^{-4}\ m^2$ in the presented analyses). Gawecka et al. (2020) presents detailed analyses demonstrating the need for adopting this material when simulating heat exchanger pipes using one-dimensional elements, as these do not have the correct lateral contact area with the surrounding concrete.

2.2 Pipe dimensions and arrangements

In order to investigate the effects of pipe arrangement on thermally-induced axial stresses, three different cases (1U, 2U and 3U) are considered. The arrangements of the pipes and the way water is circulated in each case are illustrated in Figure 3, noting that the pipe carrying the water up the pile is always diametrically opposite to the pipe carrying the water down the pile.

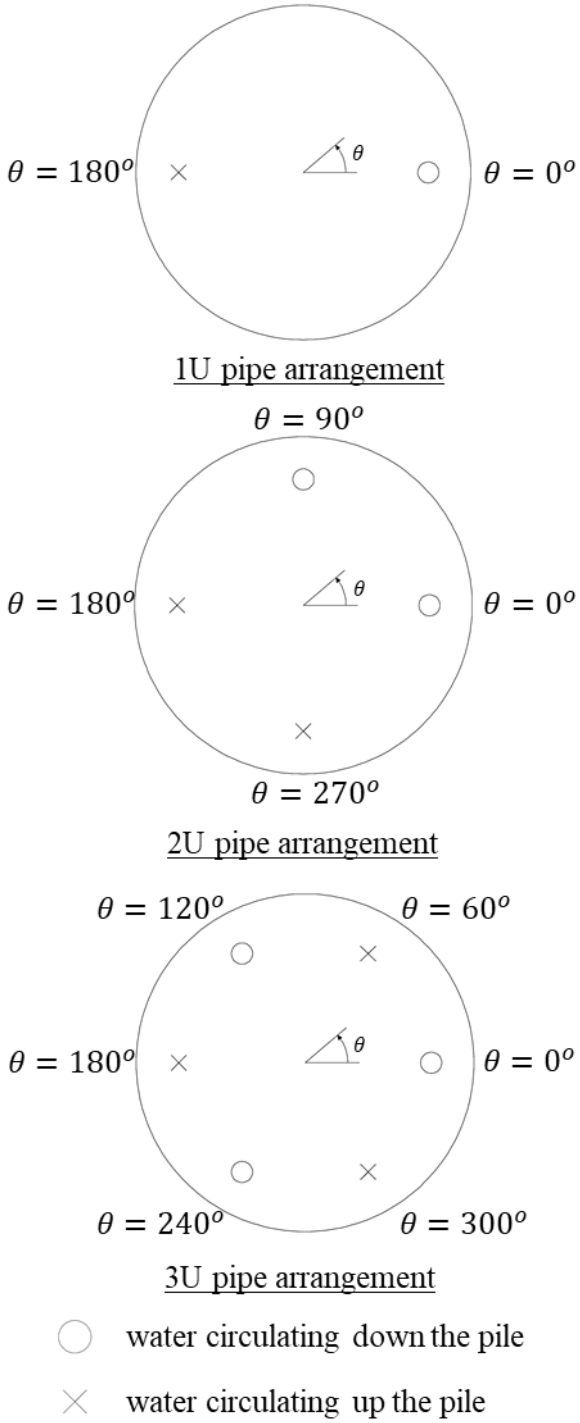

Figure 3 Illustration of 1U, 2U and 3U pipe arrangements

The distance between the pipe and the pile edge (i.e. concrete cover) is $0.07m$, as in the thermal response test reported by Loveridge et al. (2014) and subsequently adopted for numerical modelling by Gawecka et al. (2020). The pipes are modelled to have an internal diameter of $26.2mm$ and a wall thickness of $2.9mm$, corresponding to a cross-sectional area of $5.39 \times 10^{-4}\ m^2$. A flow rate of $1.032 \times 10^{-4}\ m^3/s$ for each U-loop is assumed, corresponding to a flow velocity of $0.191\ m/s$ (Loveridge et al., 2014; Gawecka et al., 2020).

2.3 Initial and boundary conditions

Due to the nature of the analyses, displacement, hydraulic and thermal boundary conditions are required. For displacement boundary conditions, the bottom of the mesh is restricted from moving in all directions, while the far cylindrical boundary is restricted from moving in the radial direction. In terms of hydraulic boundary conditions, there is no change in pore water pressure from the initial condition at the top and bottom boundaries of the mesh, and no water flow is allowed across the far cylindrical boundary. Lastly, thermal boundary conditions are prescribed such that there is no change in temperature from the initial condition at all boundaries of the mesh (except the top of the pile which is simulated as being insulated). The ground water table is assumed to be at the ground surface and the initial pore water pressure profile is assumed to be underdrained, as it typically occurs in London, consistent with the adopted non-linear permeability model (see Section 2.4) and is shown in Figure 4(a). The adopted K_0 profile (Figure 4(b)) and the initial ground temperature (19.5^oC) are similar to those adopted in Gawecka et al. (2017).

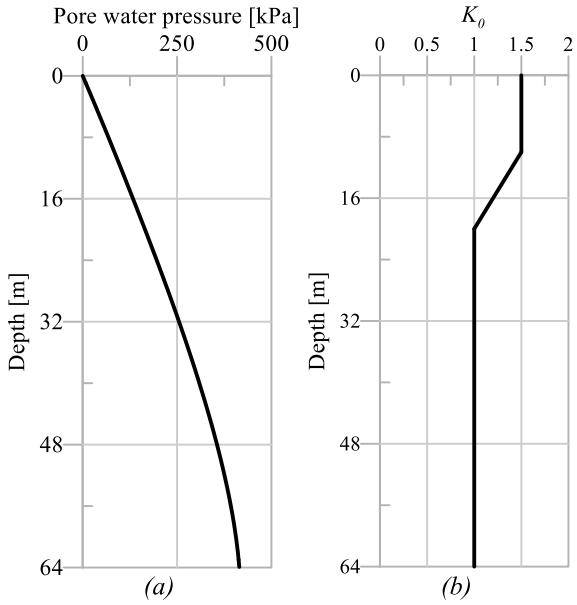

Figure 4 (a) Initial pore water pressure profile and (b) K_0 profile

2.4 Material models and properties

The behaviour of the London Clay is modelled as non-linear elasto-plastic, using a Mohr-Coulomb failure surface coupled with the Imperial College Generalised Small-Strain Stiffness (IC.G3S) model, the formulation of which is summarised in Appendix A (see Measham et al. (2014) and Taborda et al. (2016) for additional details). In terms of its hydraulic behaviour, a non-linear permeability model, where this property is a function of the mean effective stress, is adopted: $k = k_0 e^{-Bp'}$, where k_0 and B are model parameters and p' is the mean effective stress. Tables 1 and 2 report all the adopted material properties for London Clay and concrete, respectively, which are identical to those used by Gawecka et al. (2017). The heat exchanger pipes within the pile, as outlined in Table 3, are modelled with a very low stiffness and the same coefficient of thermal expansion as that adopted for the concrete pile, meaning that the mechanical properties of the pipes do not affect the distribution of thermally-induced axial stresses. The TEM surrounding the heat exchanger pipes is also modelled as a linear elastic material and has material properties identical to the ones adopted for the concrete pile, with the exception of its thermal conductivity, for which a value of 4.5 W/mK, obtained based on an empirical relationship with the internal pipe diameter, is used, and volumetric heat capacity,

for which a value of 1 kJ/m^3K is used (Gawecka et al., 2020). Note that the volumetric heat capacity of water ($\rho_w C_w$) is modelled to be 4190 kJ/m^3K.

Mohr-Coulomb strength properties	
c'	5.0 kPa
ϕ'	25.0^o
ψ'	12.5^o
Small-strain stiffness properties	
G_{ref}	51743.55 kPa
p'_{ref}	100 kPa
m_G	1.0
m_K	1.0
a	0.000056
b	0.9
$R_{G,min}$	0.06450
G_{min}	2667 kPa
K_{ref}	26692.73 kPa
r	0.000127
s	1.8
$R_{K,min}$	0.13275
K_{min}	5000 kPa
Thermal and thermo-mechanical properties	
γ_s	20.0 kN/m^3
α_s	1.7×10^{-5} m/mK
α_f	6.9×10^{-5} m/mK
K_f	2.2 GPa
ρC_p	1820 kJ/m^3K
λ	1.79 W/mK
Hydraulic properties	
k_0	1.0×10^{-10} m/s
B	0.0023 $/kPa$

Table 1 Material properties for London Clay

Linear material properties	
E	40×10^6 kPa
μ	0.3
Thermal and thermo-mechanical properties	
γ_s	24.0 kN/m^3
α_s	8.5×10^{-6} m/mK
ρC_p	1920 kJ/m^3K
λ	2.33 W/mK

Table 2 Material properties for the concrete thermo-active pile

Linear material properties	
E	1×10^3 kPa
Thermal and thermo-mechanical properties	
α_s	8.5×10^{-6} m/mK

ρC_p	$4190\ kJ/m^3K$
λ	$0.6\ W/mK$

Table 3 Material properties for the heat exchanger pipes

2.5 Modelling sequence

In order to simulate the realistic conditions that a thermo-active pile is likely to be subjected to, a mechanical load is applied before hot water is circulated through the pipes. It is assumed that the thermo-active pile is subjected to its service load, which corresponds to a factor of safety of 2.6 applied to its capacity at failure. These are estimated to be about $1800\ kN$ and $2900\ kN$ for the $600mm$ and $900mm$ diameter piles, respectively, using the α-method with $\alpha = 0.5$ and $S_u = 60 + 8z$ (as adopted in GSHPA (2012)).

Following the application of loading, full dissipation of excess pore water pressures in the surrounding soil is allowed to take place before water is circulated through the pipes at the desired velocity ($0.191\ m/s$) to isolate the effects of the heat exchange from those arising from the loading phase (hence, the thermally-induced stresses presented henceforth represent the stress changes that occur since the start of heating). The distribution of axial stresses along both the $600mm$ and $900mm$ piles just before the start of heating is shown in Figure 5. The heating of the thermo-active pile is simulated by injecting hot water at a temperature of 39.5^oC (which corresponds to a ΔT of 20^oC) for a duration of 5 months, during which the time-dependent thermally-induced axial stresses within the pile are monitored. The circulation of hot water is modelled by applying a constant temperature boundary condition of $T = 39.5^oC$ at the pipe inlet(s) and a coupled thermo-hydraulic boundary condition (Cui et al., 2016) at the pipe outlet(s) to allow removal of energy corresponding to the water flowing out of the mesh. The Petrov-Galerkin FE method (Cui et al., 2018a) is adopted for the pipes to eliminate the numerical instability associated with the modelling of an advection-dominated heat flux using the Galerkin FE method. It is appreciated that heating the thermo-active pile with a fixed inlet temperature is a simplified representation of the thermal load, as under realistic operational conditions this quantity is likely to be time-dependent. This approach is adopted to facilitate the comparison between the results of the analyses with current design charts, in which the heating of a pile is only given as a temperature change. Moreover, the application of a fixed inlet temperature ensures that any transient response obtained for the pile is exclusively due to the transient soil response arising from the simulated heat transfer mechanisms. Note that the stiffness of the London Clay is reset to its maximum value by setting the values of the deviatoric strain (E_d) and volumetric strain (ε_{vol}), used to calculate the tangent shear (G_{tan}) and bulk (K_{tan}) stiffnesses respectively (see Appendix A for the employed model equations), to zero just before the hot water is injected, to account for the increase in stiffness upon reversal of the loading direction induced by the increase in temperature, as discussed in Gawecka et al. (2017).

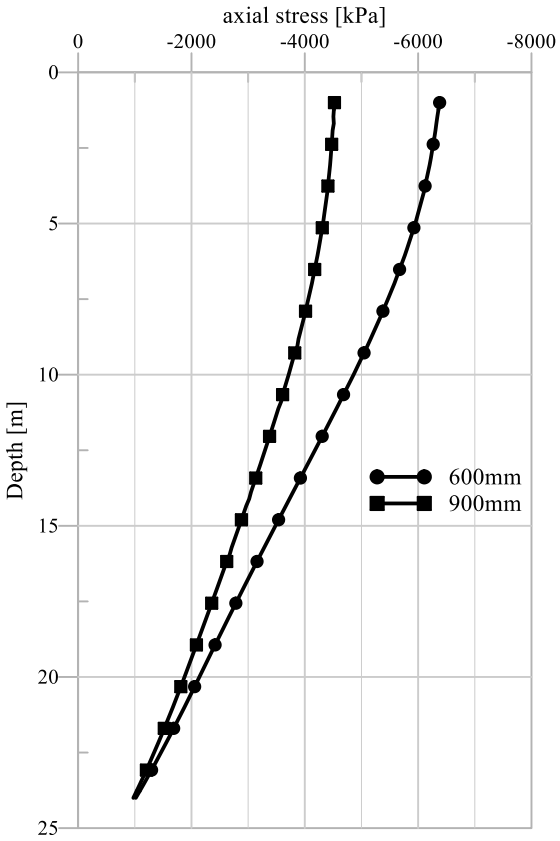

Figure 5 Distribution of axial stresses along the $600mm$ and $900mm$ piles before the start of heating

2.6 Thermo-mechanical pile response

When heat is injected into a thermo-active pile, its temperature increases. Consequently, it expands and compressive axial stresses develop within the pile due to the restraint from the soil, which, being subjected to lower temperature changes, expands less than the pile. As heat is transferred to the pile from the hot water circulating through the pipes, the temperature distribution is non-uniform within the pile, meaning that thermally-induced axial stresses, denoted by σ_T, are not only a function of time, but also vary with position within the pile cross-section and depth. To simplify the interpretation of the thermo-mechanical behaviour of the pile, the cross-sectionally averaged σ_T, denoted by $\overline{\sigma_T}$, is used. This quantity is obtained by integrating σ_T over the pile section, thus obtaining the axial force, and then dividing by the cross-sectional area of the pile. Moreover, the maximum $\overline{\sigma_T}$ over the pile length is denoted by $\overline{\sigma_T}_{max}$, which is therefore only a function of time.

Figures 6 to 8 show the distributions of temperature change and thermally-induced axial stresses within the $900mm$ pile cross-section for 1U, 2U and 3U pipe arrangements, respectively, while the corresponding figures for the $600mm$ pile are reported in Appendix B. Note that the small circles surrounding the positions of the pipes define the areas of the cross-section occupied by the TEM (see Section 2.4). Moreover, the pile cross-sections in these figures are plotted at the time instants and elevations where the value of $\overline{\sigma_T}$ is the largest over the pile length (i.e. the position at which $\overline{\sigma_T}_{max}$ occurs). For all cases, this has been observed to correspond to a depth of around $17m$ (see Figure 9), which is below the mid-depth of the pile, due to the modelled dependency on the value of mean effective stress of the stiffness of

the London Clay (see Appendix A). Similar trends have been observed by Laloui et al. (2006), Yavari et al. (2014) and Gawecka et al. (2017).

As expected, the temperature distributions are highly non-uniform, with the temperature of the regions closer to the pipes being considerably higher. Consequently, the larger thermal expansion of the concrete in these locations leads to the spatial distribution of the thermally-induced axial stresses following similar patterns as those of the temperature changes. Moreover, with the increase in the number of U-loops, the temperature field clearly becomes more uniform and is characterised by larger average temperatures and, consequently, larger axial stresses. As expected, the time instant at which the peak stress occurs is also observed to reduce with the increase in the number of U-loops due to the associated faster increase in pile temperature.

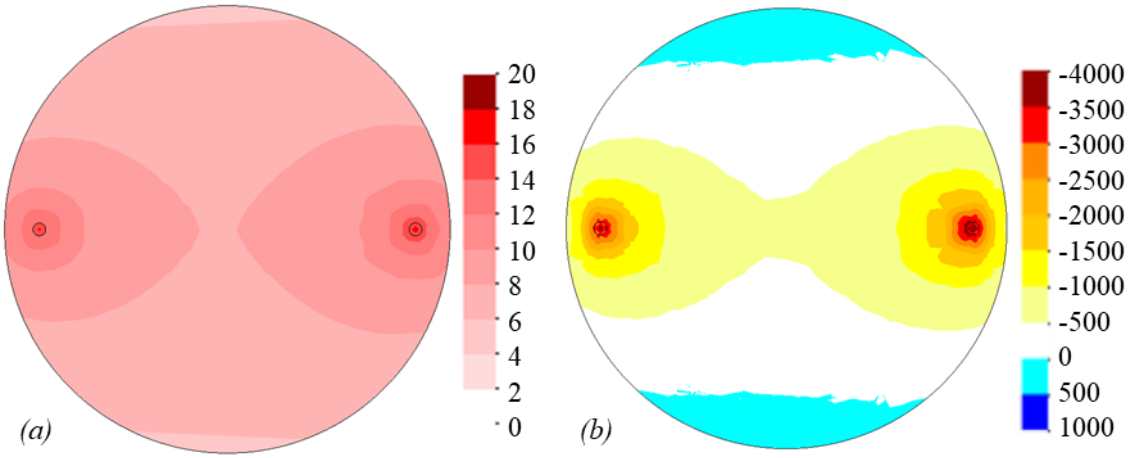

Figure 6 Distribution of (a) temperature change $[°C]$ and (b) thermally-induced axial stresses σ_T $[kPa]$ within the cross-section of the $900mm$ pile with 1U pipe arrangement at $t = 8\ days$ and $17m$ depth

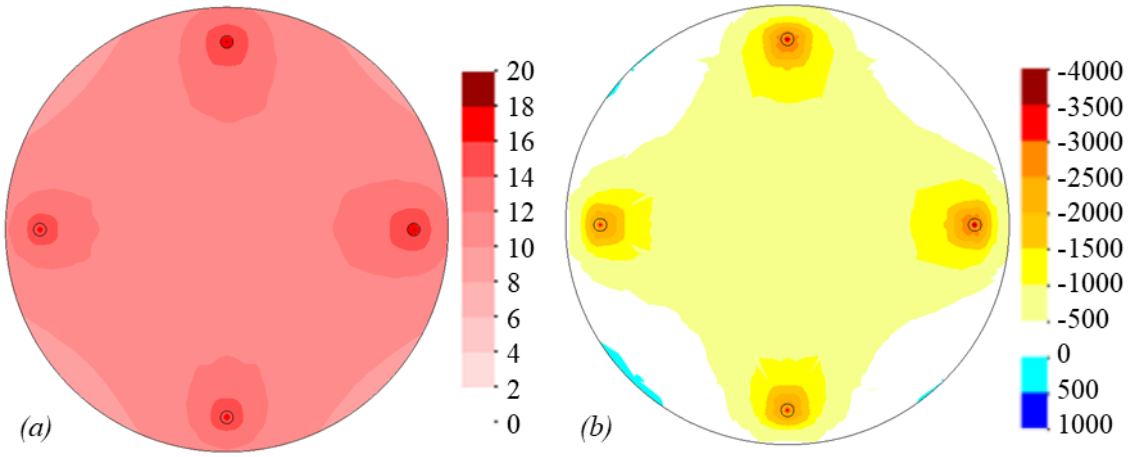

Figure 7 Distribution of (a) temperature change $[°C]$ and (b) thermally-induced axial stresses σ_T $[kPa]$ within the cross-section of the $900mm$ pile with 2U pipe arrangement at $t = 5\ days$ and $17m$ depth

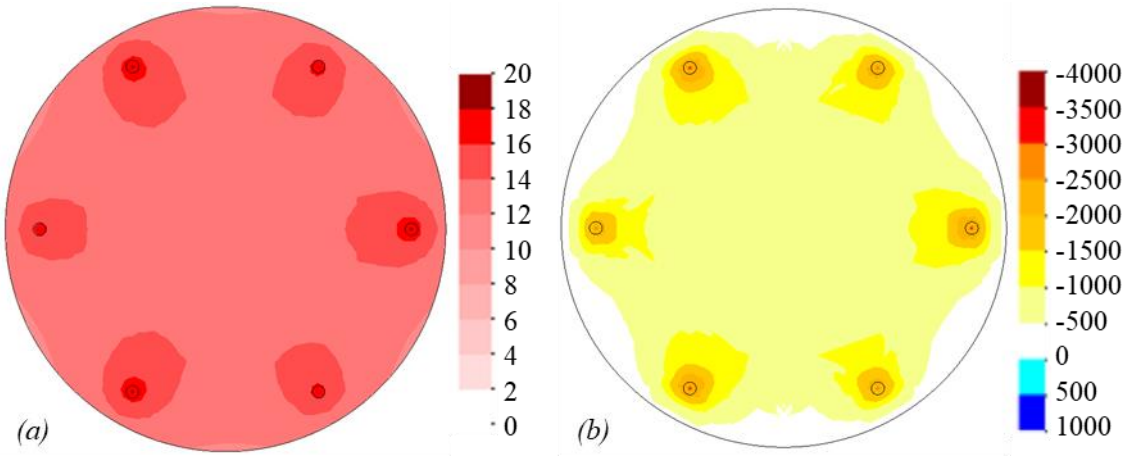

Figure 8 Distribution of (a) temperature change $[°C]$ and (b) thermally-induced axial stresses σ_T $[kPa]$ within the cross-section of the $900mm$ pile with 3U pipe arrangement at $t = 4\ days$ and $17m$ depth

Figure 9 plots the distribution of $\overline{\sigma_T}$ along the pile length for the analyses on the $900mm$ pile, at the time instants when the corresponding values of $\overline{\sigma_T}_{max}$ are the largest over the 5 months of heating (the corresponding figure for the analyses on the $600mm$ pile is given in Appendix B). The evolutions of $\overline{\sigma_T}_{max}$ with time for the analyses on the $600mm$ and $900mm$ piles over the five months of heating are displayed in Figure 10, where the previous considerations on the temperature distributions are confirmed, i.e. larger values of axial stress develop for greater number of U-loops. For the $900mm$ pile, the peak $\overline{\sigma_T}_{max}$ increases by 39.0% when the number of U-loops increases from one to two, while increasing the number of U-loops from two to three only increases the peak $\overline{\sigma_T}_{max}$ by 15.6%. The equivalent figures for the $600mm$ pile are 34.0% and 11.4% respectively. This implies that increasing the number of U-loops does not lead to a directly proportional increase in thermally-induced axial stresses, which is expected as the heat transfer from the pipes to the concrete pile depends on the thermal gradient between these two elements, which is reduced by a higher average pile temperature when the number of U-loops increases. Moreover, as seen in Figure 10, for the same number of U-loops, reducing the pile diameter from $900mm$ to $600mm$ increases the peak $\overline{\sigma_T}_{max}$ significantly (106.9%, 99.5% and 92.3% for 1U, 2U and 3U respectively). In the $600mm$ pile, the smaller distance between the heat exchanger pipes leads to larger average temperatures (see Appendix B) and hence, larger thermally-induced axial stresses. It is interesting to note that the peak values of $\overline{\sigma_T}_{max}$ are substantial, corresponding to about 30%-50% ($600mm$ pile) and 20%-30% ($900mm$ pile) of the axial stress values due to static loading at the same depth (approximately $17m$). This further demonstrates the need to take account of thermal loading when designing this type of structures. Furthermore, Figure 10 also demonstrates the highly transient nature of this type of problem. As hot water is injected into the pile and the temperature increases, the concrete expands and axial stresses increase due to the restraint applied from the surrounding soil. As time progresses, the soil temperature increases and compressive excess pore water pressures are induced since the coefficient of thermal expansion of the pore fluid is larger than that of the soil. Thermally-induced pore water pressures reduce the effective stresses, leading to tensile mechanical volumetric strains, or swelling, in the soil, in addition to its thermal expansion due to heating. This expansion reduces the restraint imposed on the pile, leading to a reduction in axial stresses with time after reaching a peak. Note that this transient behaviour was also observed in previous studies of thermo-active piles (e.g. Gawecka et al., 2017; Liu et al., 2019) and thermo-active retaining walls (Sailer et al., 2019). Gawecka et al. (2017) investigated the behaviour of a thermo-active pile when subjected

to heating and cooling by conducting analyses with different levels of coupling, and concluded that thermally-induced axial stresses are significantly overestimated if heat transfer within the soil is not modelled, as in such a scenario the soil does not contract or expand, imposing the greatest restriction onto the pile. Moreover, it was found that stresses are slightly underestimated if an undrained analysis is performed (i.e. seepage is not modelled). In fact, in analyses where coupled consolidation is modelled, it has been observed that the dissipation of excess pore water pressures and the associated contraction of the material surrounding the pile lead to an increase in the restraint imposed by the soil onto the pile and therefore to higher stresses. In undrained analyses, the absence of such phenomenon explains the abovementioned underestimation of thermally-induced axial stresses. These findings highlighted the importance of full THM coupling in the simulation of transient behaviour. Furthermore, it can be observed in Figure 10 that, during the transient stage, the initial rate of $\overline{\sigma_T}_{max}$ reduction increases with the number of U-loops for both $600mm$ and $900mm$ piles, due to the faster heat transfer to the soil inducing a greater thermal expansion. With time, the rate of $\overline{\sigma_T}_{max}$ reduction decreases, and, after five months of heating, the evolutions of $\overline{\sigma_T}_{max}$ have almost stabilised. Clearly, the reduction in $\overline{\sigma_T}_{max}$ during the transient stage increases with peak $\overline{\sigma_T}_{max}$ for all the analyses, and the $\overline{\sigma_T}_{max}$ after five months of heating are only around half of the peak $\overline{\sigma_T}_{max}$.

The transient behaviour described above can only be captured adequately by performing fully-coupled thermo-hydro-mechanical analyses, as it requires the time-dependent temperature and pore water pressure changes within the soil to be modelled, as well as the effects of differential thermal expansion between the soil skeleton and the pore fluid.

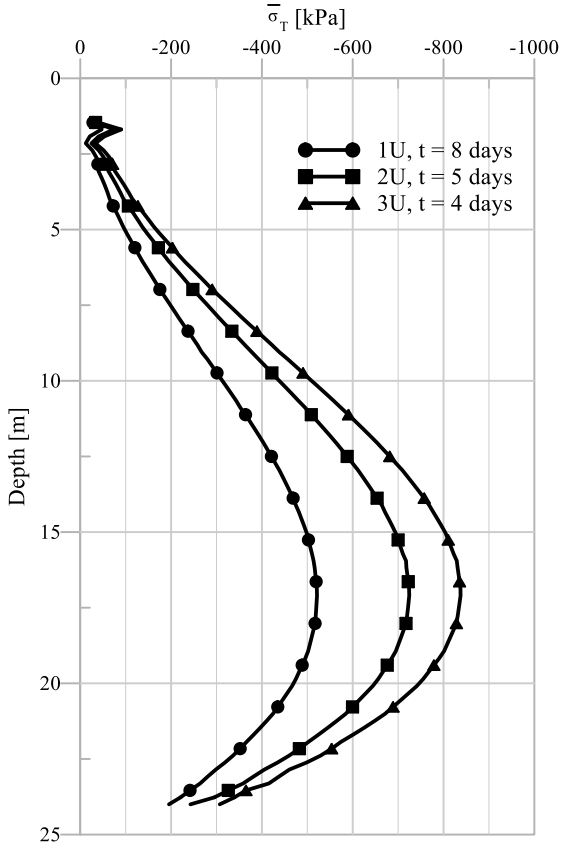

Figure 9 Distribution of $\overline{\sigma_T}$ along the pile length for the analyses on the $900mm$ pile

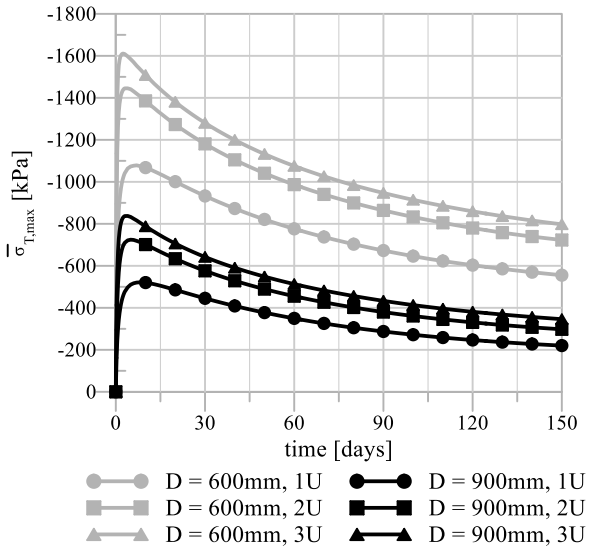

Figure 10 Evolution of $\overline{\sigma_T}_{max}$ with time for the analyses on the $600mm$ and $900mm$ piles

When comparing the results from different analyses, it is found that the time to reach peak $\overline{\sigma_T}_{max}$ is related to the volume of concrete each heat source is required to heat up – measured herein by the number of heat sources normalised by the pile circumference – and the rate of heat transfer to the soil. In effect, Figure 11 demonstrates that, for all the cases considered, a unique relationship between these two quantities exists. Note that each U-loop is considered as two heat sources.

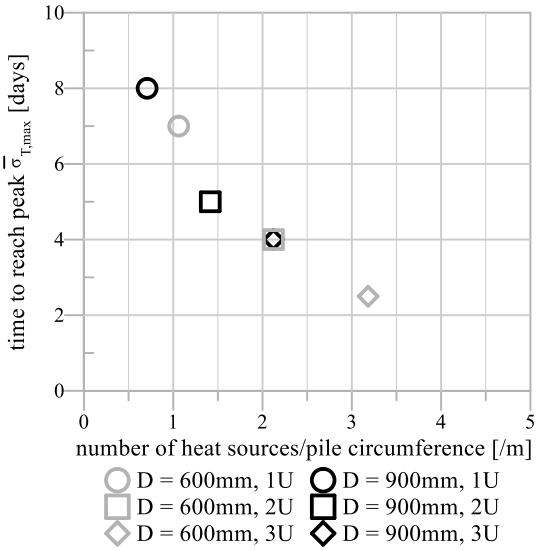

Figure 11 Ratio of number of heat sources to pile circumference versus time to reach peak $\overline{\sigma_T}_{max}$

The importance of transient behaviour is further illustrated in Figure 12, where the obtained values of peak $\overline{\sigma_T}_{max}$ are compared to those indicated by the current design charts proposed by GSHPA (2012) for the same pile diameters, loading conditions, and temperature changes (20^oC). Clearly, it can be observed that the peak values of $\overline{\sigma_T}_{max}$ obtained from the 3D analyses, based on which the pile would be designed, are significantly larger (up to 282%) than those suggested by the design charts, though the differences seem to reduce significantly with time. Indeed, the maximum difference between the values in the design charts and the numerical prediction reduces to 58% at the end of the simulation period. The large differences

are possibly due to the different modelling approaches adopted, since the design charts in GSHPA (2012) have been developed using a load transfer method (t-z method), which is unable to model the non-isothermal response of soil and, hence, account for the transient response of the thermo-active pile.

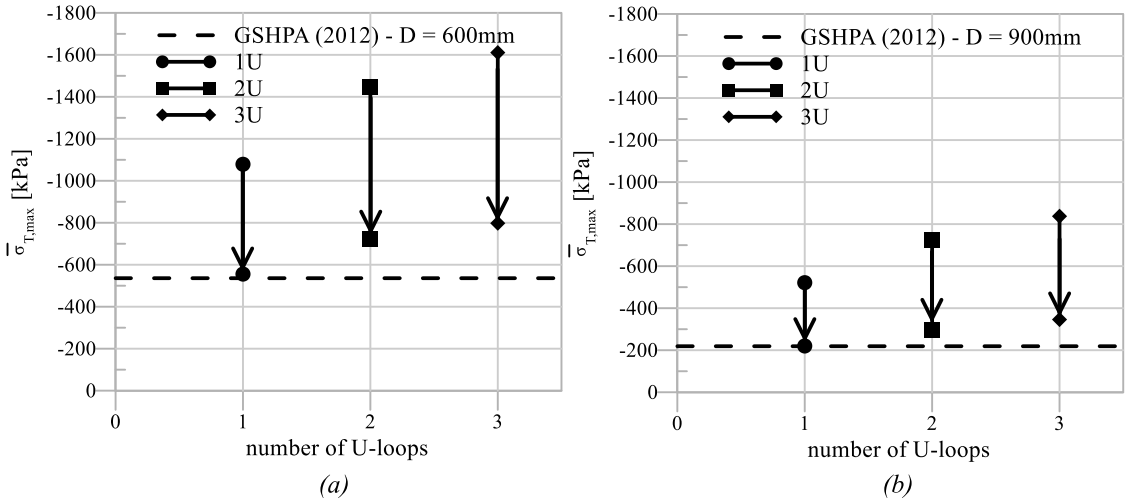

Figure 12 Peak $\overline{\sigma_T}_{max}$ and transient behaviour plotted with the recommended values from the design chart by GSHPA (2012) for piles of $25m$ in length and diameter of (a) $600mm$ and (b) $900mm$

It is also interesting to compare the evolutions of $\overline{\sigma_T}_{max}$ with time obtained from the 3D analyses with those calculated using "conventional" axisymmetric coupled THM analyses, where the entire volume of the pile is subjected to a change in temperature of 20^oC. In Appendix C, the results of two scenarios are shown using this type of approach: (I) the pile temperature changes instantaneously by 20^oC at the start of the analysis and (II) the pile temperature is assumed to vary linearly from 19.5^oC to 39.5^oC in one month, and is then held constant at 39.5^oC for four months). Clearly, a severe limitation of this approach is highlighted by the fact that a single curve is obtained for each scenario and each diameter as the number of U-loops in the pile are not taken into account. Moreover, as expected, scenario (I) leads to a very large overestimation of the peak axial stress, particularly for pipe configurations consisting of a single U-loop, where the heat transfer between the heat exchanger pipes and the pile takes place at a slower rate. Conversely, scenario (II) displays a transient response which is significantly different from that observed in the 3D analyses. In terms of peak axial stresses, the "conventional" approach is conservative for some pipe configurations (those with lower number of U-loops, i.e. lower heating rate) and unconservative for others (those with a larger number of U-loops, i.e. higher heating rate), with this split changing with the pile diameter. This highlights the importance of modelling accurately the heating mechanisms present in a thermo-active pile by including the discrete locations of the heat exchanger pipes in the cross-section of the pile and reinforces the need for a new methodology for simulating thermo-active piles in axisymmetric analyses.

3 A SIMPLIFIED METHOD

Given the high computational cost of three-dimensional analyses and the complexity inherent in the simulation of heat exchanger pipes (the need to use e.g. Petrov-Galerkin FE), a simplified method to estimate thermally-induced axial stresses is proposed that requires solely a 2D thermal analysis combined with an axisymmetric coupled THM analysis. The 3D analyses

presented in the previous section are used as benchmark to demonstrate the excellent accuracy of the devised method.

3.1 The method

The fundamental idea behind the proposed simplified method is to obtain thermally-induced axial stresses within a thermo-active pile using an axisymmetric coupled THM analysis, where the heating or cooling of the pile is simulated using a time-dependent prescribed temperature ($T_{tbc}(t)$) as a thermal boundary condition. This temperature $T_{tbc}(t)$ is applied at a radial distance equal to that of the pipes (i.e. $r = r_{pipes}$) and its value is taken as the time-dependent average temperature at $r = r_{pipes}$ calculated using a 2D thermal analysis of the cross-section of the pile where the discrete nature and precise location of the heat exchanger pipes is modelled. The steps required to determine the thermally-induced axial stresses using the proposed simplified method are outlined below.

Step 1: Determine the thermal boundary condition for the 2D thermal analysis

In order to approximate the time-dependent temperature field in the cross-section of a thermo-active pile, a 2D thermal analysis has to be conducted. A constant temperature thermal boundary condition is applied at the locations where the pipes are located in the real problem, and the constant temperatures that are applied, $T_{in,mid}$ and $T_{out,mid}$, can be estimated from the temperatures at the inlet (T_{in}) and outlet (T_{out}) of each U-loop, where T_{in} is the design inlet temperature, while T_{out} can be estimated using the following equation:

$$T_{out} = T_{in} - \frac{\Delta E \cdot L}{n_{U-loops} \cdot \rho_w C_w \cdot Q} \quad (1)$$

where ΔE is an assumed power injected to/extracted from the pile per unit pile length [kW/m], L is the pile length [m], $n_{U-loops}$ is the number of U-loops in the thermo-active pile, $\rho_w C_w$ [kJ/m^3K] is the volumetric heat capacity of water, and Q [m^3/s] is the flow rate of the water. Naturally, the real injected or extracted power is unknown without conducting a field test or a 3D FE analysis similar to those carried out in the previous section, where water flowing through heat exchanger pipes is explicitly simulated. Therefore, a constant injection rate of $35\ W$ per m^2 of earth-contact area can be assumed, as suggested by Brandl (2006) for piles with diameters $\geq 600mm$ (this would result, for example, in a heat injection rate per unit length (ΔE) of $66\ W/m$ for a $600mm$ diameter pile and $99\ W/m$ for a $900mm$ diameter pile, which are well within the range of power outputs of thermo-active piles reported in the literature, as summarised by Bourne-Webb (2013) and Faizal et al. (2016)). However, it should be appreciated that in the context of the proposed 2D thermal analysis, ΔE is solely used to provide an initial estimate for T_{out}, and subsequently $T_{in,mid}$ and $T_{out,mid}$ using Equations (2) and (3), and not as an actual measure of the transferred energy. In effect, these are then applied as thermal boundary conditions, which will control the amount of heat being transferred to the pile and the surrounding ground. Therefore, the adoption of ΔE is justified as a form of obtaining more realistic temperature profiles along the pipes that can be used to establish the boundary conditions in the 2D thermal analysis. As will be demonstrated in Section 3.4, the output of the proposed method is relatively unaffected by the adopted value of ΔE, provided reasonable values are used. Note that it is not a requirement of the proposed method to have a fixed inlet temperature. In effect, if a transient inlet temperature is to be adopted, including

cycles of heating and cooling, T_{in} would be a function of time and T_{out} would still be determined using Equation (1).

By assuming that the temperatures within the pipes vary linearly with depth, $T_{in,mid}$ and $T_{out,mid}$ can be estimated as:

$$T_{in,mid} = T_{in} - (T_{in} - T_{out}) \times \frac{1}{4} \quad (2)$$

$$T_{out,mid} = T_{in} - (T_{in} - T_{out}) \times \frac{3}{4} \quad (3)$$

Step 2: Conduct the 2D thermal analysis

Adopting the constant temperature boundary condition as explained in Step 1, the 2D thermal analysis is conducted to simulate the evolution of the temperature field over the entire duration of thermal loading. Note that the simulation of TEM should be adopted at the locations where the pipes are located.

Step 3: Determine the $T_{tbc}(t)$ that is used as a prescribed temperature boundary condition for the axisymmetric coupled THM analysis

Following the 2D thermal analysis described in Step 2, a time-dependent temperature field is obtained. For each time step of the 2D thermal analysis, the temperature distribution along the circumference with $r = r_{pipes}$ is extracted. Using the mean value theorem for integrals, the average temperature at $r = r_{pipes}$ is obtained for each of the time instants, generating the time-dependent temperature $T_{tbc}(t)$, which is to be applied as a thermal boundary condition in the axisymmetric coupled THM analysis, thus simplifying significantly the complexity of the simulated problem by removing the need to explicitly model heat exchanger pipes.

Step 4: Conduct the axisymmetric coupled THM analysis

The axisymmetric coupled THM analysis is conducted by applying the time-dependent temperature $T_{tbc}(t)$ obtained in Step 3 at $r = r_{pipes}$, adopting appropriate material properties for the pile and the surrounding soil, as well as initial and boundary conditions (e.g. if a restraint to the pile head exists, such as when simulating the existence of a superstructure, then appropriate boundary condition should be applied at the pile head in the axisymmetric coupled THM analysis to reflect this). Note that the simulation of TEM is not necessary in axisymmetric analyses. The thermally-induced axial stresses can then be determined from the results of this axisymmetric analysis.

3.2 Example

The proposed simplified method is demonstrated using the case for the $900mm$ thermo-active pile with a single U-loop. For the 2D thermal analysis, a finite element mesh featuring discretisation and dimensions identical to that used in the 3D analysis for the pile and London Clay is adopted, using eight-noded quadrilateral elements with one temperature degree of freedom at each node. The design inlet temperature T_{in} is 39.5^oC, Equation (1) then yields $T_{out} = 33.8^oC$ for $\Delta E = 99\ W/m$ (based on the assumption of $35\ W$ per m^2 of earth-contact area), $L = 25m$, $n_{U-loops} = 1$, $\rho_w C_w = 4190\ kJ/m^3K$ and $Q = 1.032 \times 10^{-4}\ m^3/s$ (i.e.

the value used in the previous section). $T_{in,mid}$ and $T_{out,mid}$ are subsequently determined to be 38.1^oC and 35.2^oC using Equations (2) and (3) respectively. The 2D thermal analysis is then conducted by applying the constant temperature thermal boundary conditions $T_{in,mid}$ and $T_{out,mid}$ at the locations where the pipes are located in the 3D 1U analysis, as illustrated in Figure 13, to simulate the evolution of the temperature field over the 150 days of heating, using the same thermal properties for the pile concrete, TEM, and the London Clay as those employed in the 3D analyses (see Tables 1 and 2).

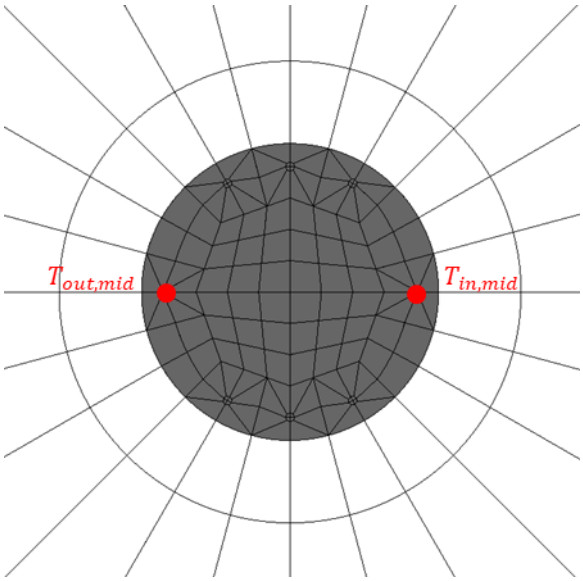

Figure 13 Illustration of the thermal boundary condition for the 2D thermal analysis

For each time step of the 2D thermal analysis, the temperature distribution along the circumference with $r = r_{pipes}$ is extracted. Figure 14 illustrates such a curve at $t = 8\ days$, where the angle θ is defined in Figure 3. As expected, for this pipe arrangement, two peaks exist at $\theta = 0°$ (water circulating down the pile) and $\theta = 180°$ (water circulating up the pile), with the temperature being highest in the former as it represents the inlet branch of the U-loop. The average temperature at $r = r_{pipes}$ is then obtained for each of the time instants, generating the time-dependent temperature $T_{tbc}(t)$ shown in Figure 15.

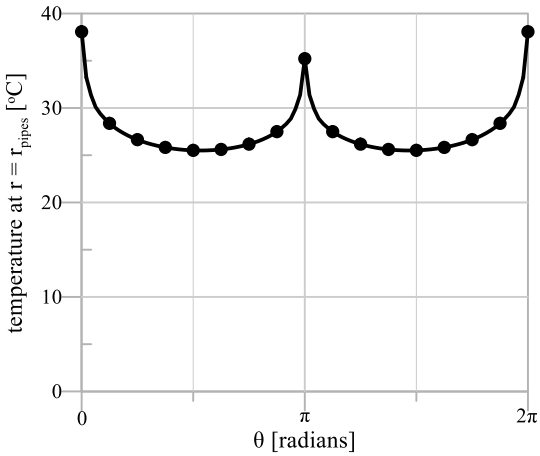

Figure 14 θ versus T curve at $r = r_{pipes}$ and $t = 8\ days$ for the 2D thermal analysis on the $900mm$ pile with 1U pipe arrangement

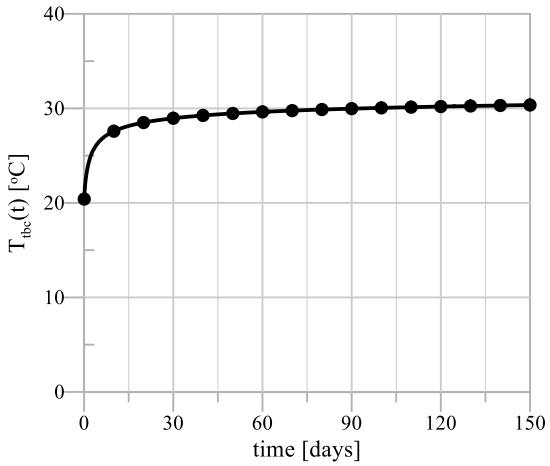

Figure 15 Time versus $T_{tbc}(t)$ for the 900mm pile with 1U pipe arrangement

The axisymmetric coupled THM analysis is then conducted by applying the time-dependent temperature $T_{tbc}(t)$ as a thermal boundary condition at $r = r_{pipes}$ (see Figure 16). In this analysis, the discretisation of the mesh (shown in Figure 16) is identical to that adopted in the 3D analyses (see Figure 1) in the $x - z$ plane, using eight-noded quadrilateral elements with two displacement and one temperature degrees of freedom at each node. For the elements discretising the London Clay, pore water pressure degrees of freedom also exist at corner nodes. The initial and boundary conditions are applied in accordance with those described in Section 2.3 for the 3D analyses, while the adopted material properties for London Clay and pile concrete are naturally the same as those listed in Tables 1 and 2.

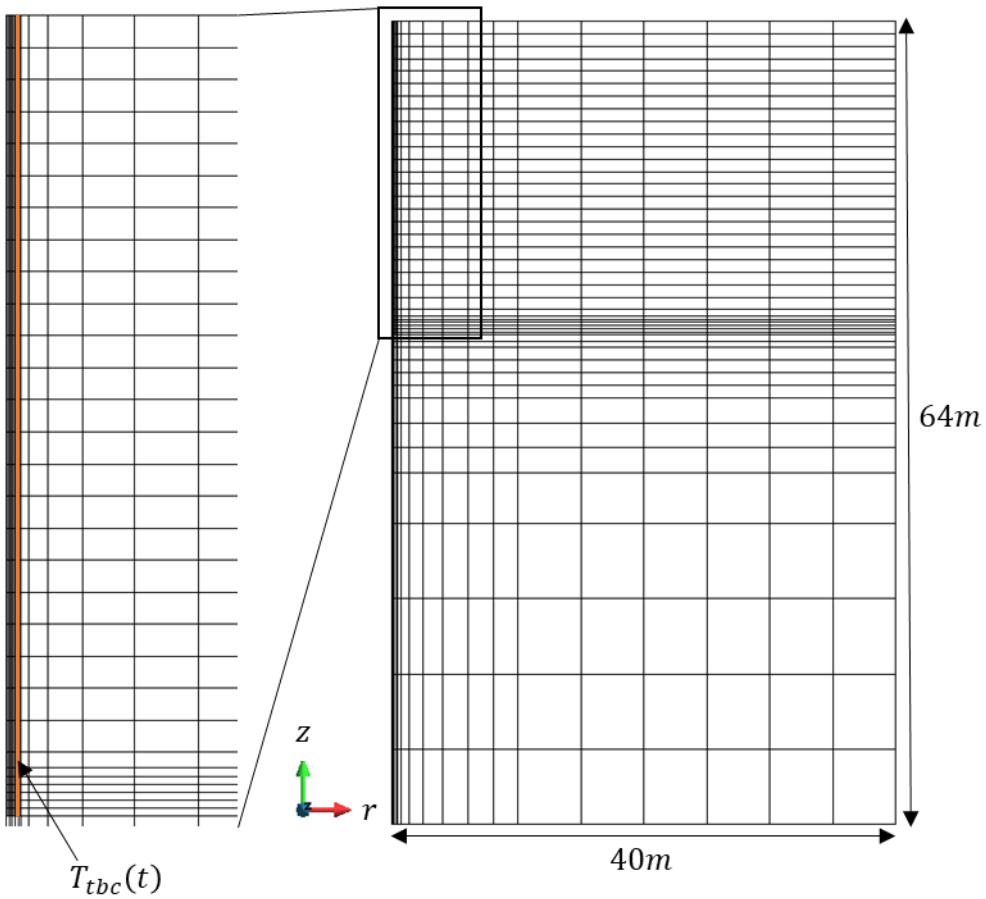

Figure 16 The axisymmetric FE mesh and the zoomed-in mesh detailing the pile (shaded in grey) and the location where $T_{tbc}(t)$ is applied within the pile (highlighted in red) for the axisymmetric analyses

3.3 Performance of the proposed method

Figure 17 compares the evolution of $\overline{\sigma_T}_{max}$ with time computed with the proposed method to those obtained from the 3D analyses described in the previous section. Table 4 reports the magnitudes of peak $\overline{\sigma_T}_{max}$ given by the proposed method and 3D analyses and the corresponding relative errors.

Clearly, the obtained results demonstrate that the proposed method is capable of predicting with good accuracy the value of peak $\overline{\sigma_T}_{max}$, the time instants at which it occurs, as well as the overall transient behaviour of each pile. Indeed, for all the analysed cases, the maximum difference in peak $\overline{\sigma_T}_{max}$ is less than 7% of the one recorded in the 3D analysis. As explained in Section 2.6, thermally-induced axial stresses are ultimately driven by temperature changes. In order to account for the accurate resemblance of the $\overline{\sigma_T}_{max}$ evolution given by the proposed method, Figures 18 and 19 compare the evolution of temperature changes simulated by the proposed method against those obtained from the 3D analyses (averaged at the corresponding radial distance from the centre of the pile using the mean value theorem for integrals) at the centre of the pile, edge of pile and $250mm$ away from the pile edge in the soil, at mid-depth of the pile, for the $600mm$ and $900mm$ piles, respectively. Clearly, as shown in Figures 18 and 19, the accurate simulation of temperatures, both within and around the thermo-active pile, demonstrates why the proposed method is capable of simulating thermally-induced axial stresses with such a high degree of accuracy.

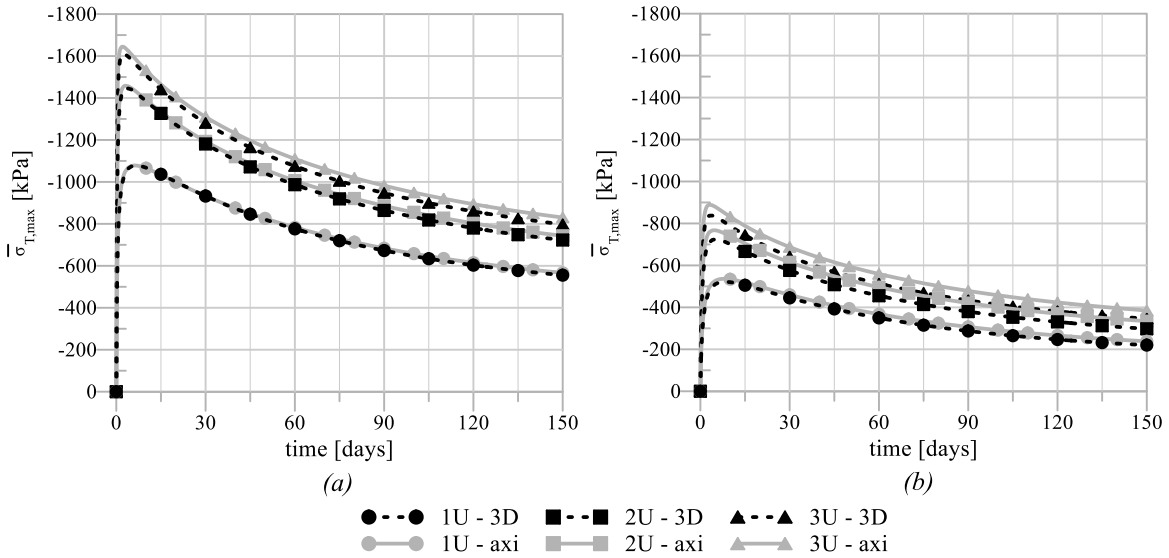

Figure 17 Evolution of $\overline{\sigma_T}_{max}$ with time estimated from the proposed method compared with results from the 3D analyses for the (a) $600mm$ and (b) $900mm$ piles

Pile diameter $[mm]$	Pipe arrangement	Peak $\overline{\sigma_T}_{max}$ [kPa]		Relative error [%]
		Proposed method	3D analysis	
600	1U	1078.5	1078.6	0.0
	2U	1458.6	1445.3	0.9

	3U	1644.5	1610.7	2.1
900	1U	536.3	521.4	2.9
	2U	767.5	724.5	5.9
	3U	889.3	837.5	6.2

Table 4 Magnitudes of peak $\overline{\sigma_T}_{max}$ given by the proposed method and 3D analyses and the corresponding relative errors

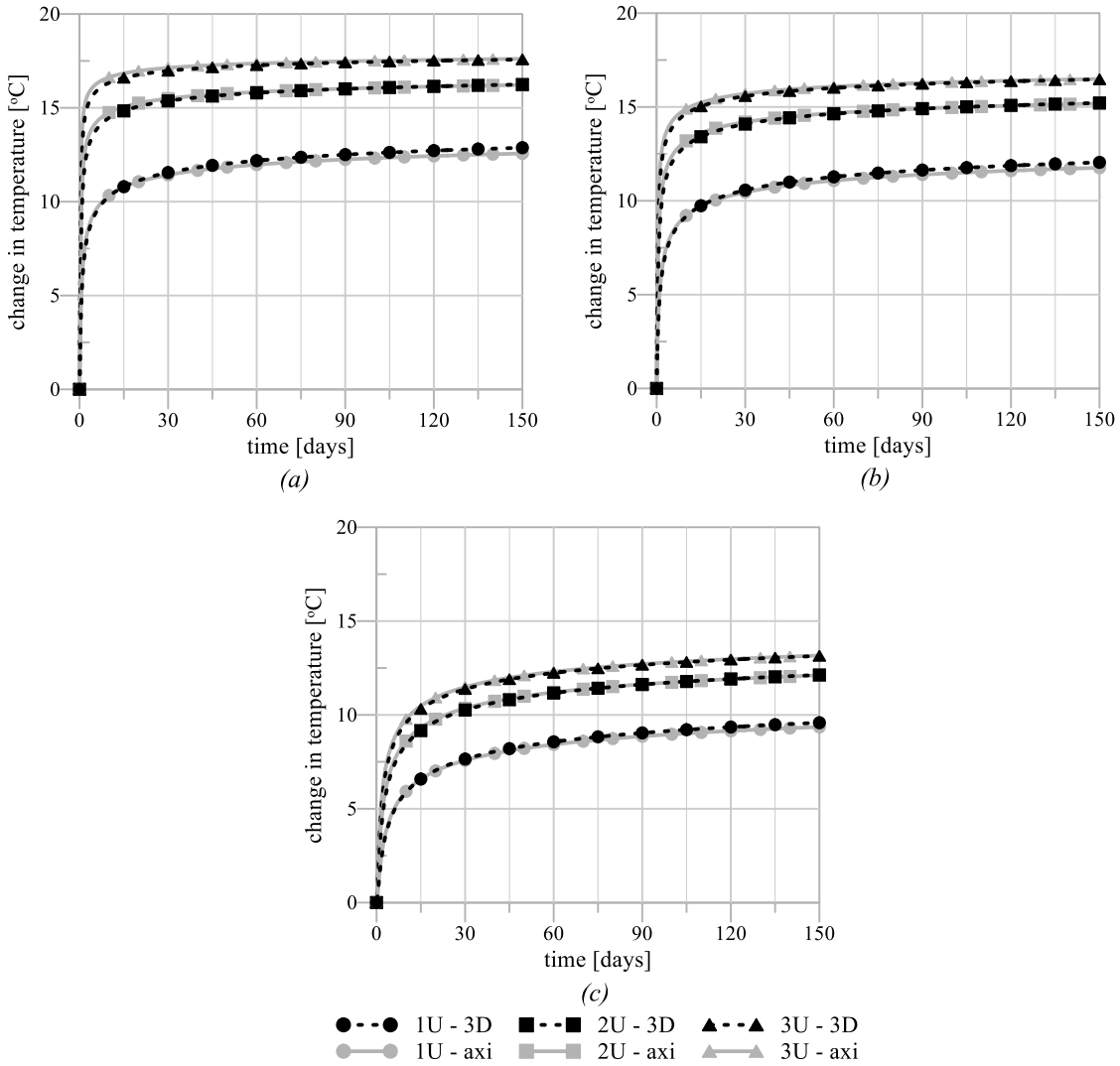

Figure 18 Evolutions of temperature changes simulated by the 3D analyses and the proposed method at (a) the centre of pile, (b) the edge of pile, and (c) $250mm$ away from the edge of pile in the soil for the $600mm$ pile

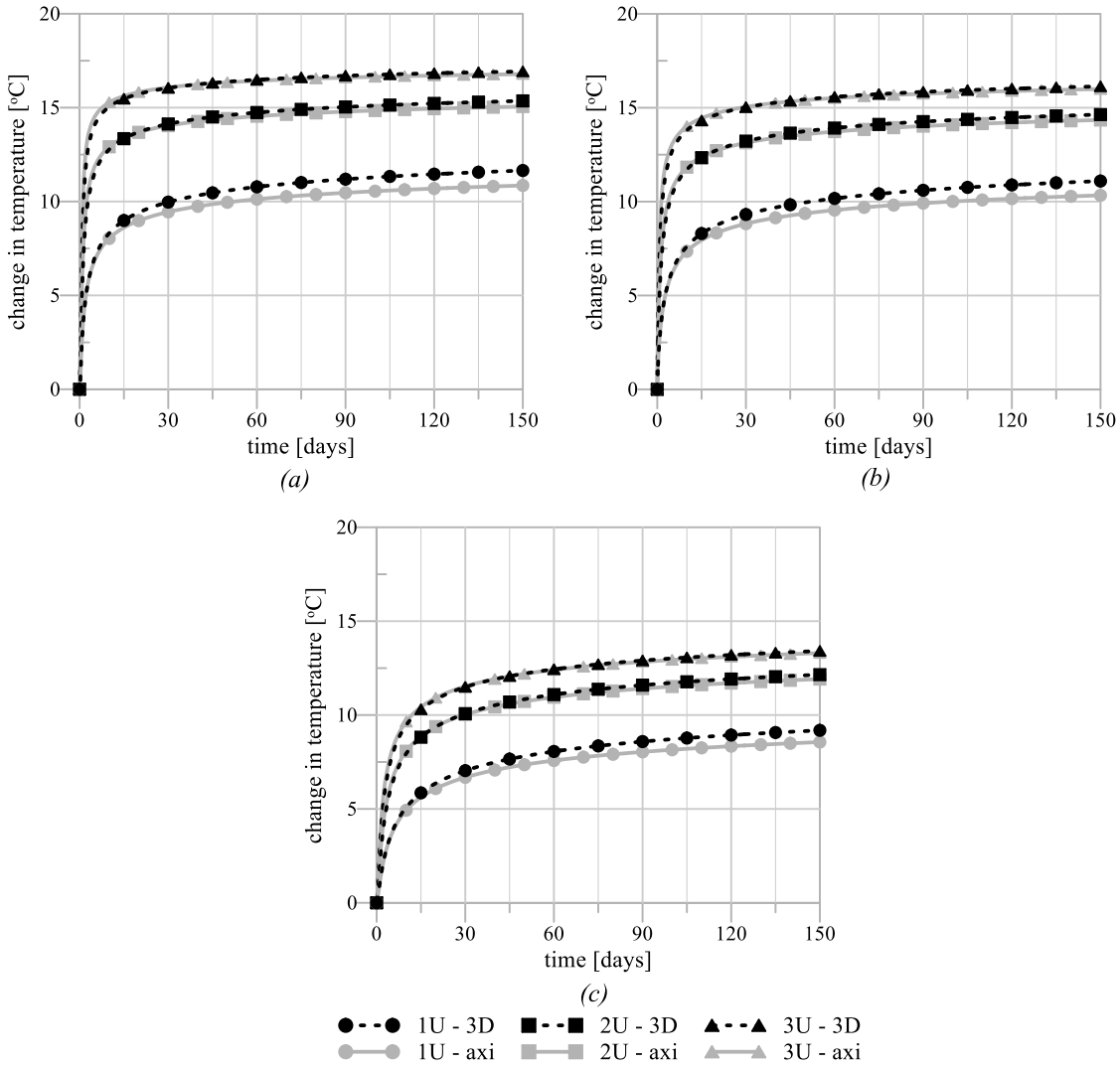

Figure 19 Evolutions of temperature changes simulated by the 3D analyses and the proposed method at (a) the centre of pile, (b) the edge of pile, and (c) $250mm$ away from the edge of pile in the soil for the $900mm$ pile

3.4 Sensitivity of the proposed method to ΔE estimation

The only source of uncertainty in the application of the proposed method arises from the need to estimate the profile of temperatures along the pipes, which is based on an assumed energy output of the pile, ΔE, in order to apply Equation 1. Given that alternative approaches could be used to estimate the value of ΔE (e.g. using local knowledge on the performance of thermo-active structures), the sensitivity of the proposed method to the value of this quantity is assessed. Thus, the proposed method is applied to the cases considered in the previous sections by assuming two extreme values for ΔE, $0\,W/m$ and $210\,W/m$. Clearly, $\Delta E = 0\,W/m$ represents the most conservative case, since it leads to the highest applied temperatures in the 2D thermal analyses (i.e. $T_{in,mid} = T_{out,mid} = T_{in}$) which are also independent of the number of U-loops. Furthermore, $\Delta E = 210\,W/m$ represents an upper bound of thermal performance of thermo-active piles reported in the literature, as summarised by Bourne-Webb (2013). The results of the analyses are given in Figure 20, while Table 5 outlines the magnitudes of peak $\overline{\sigma_T}_{max}$ and the relative reduction in the predicted values for peak $\overline{\sigma_T}_{max}$ when ΔE increases from $0\,W/m$ to $210\,W/m$.

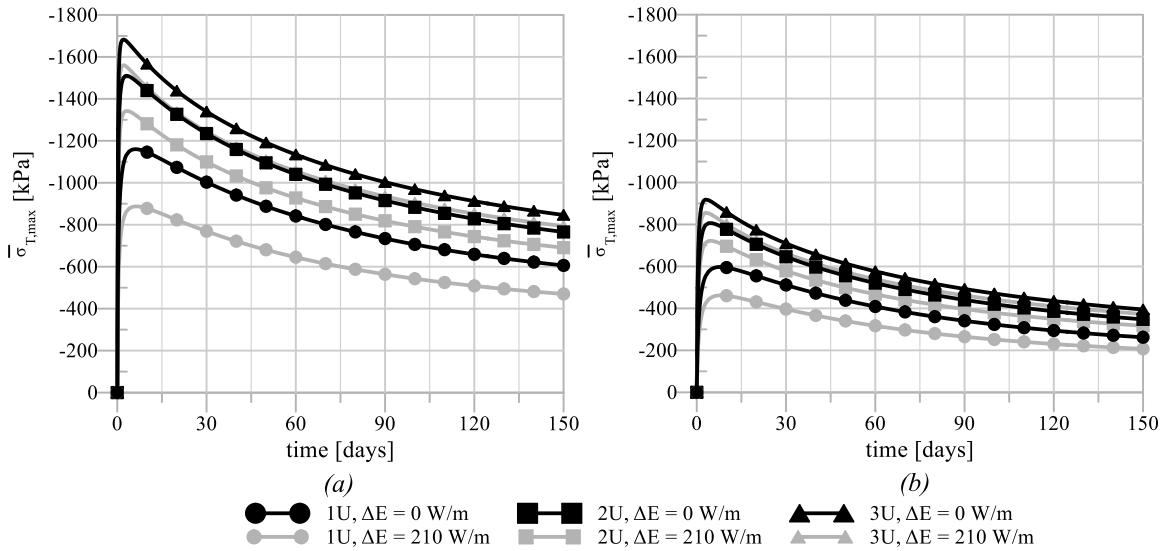

Figure 20 Evolution of $\overline{\sigma_{T}}_{max}$ with time estimated from the proposed method using $\Delta E = 0\ W/m$ and $210\ W/m$ for the (a) $600mm$ and (b) $900mm$ piles

Pile diameter $[mm]$	Pipe arrangement	Peak $\overline{\sigma_{T}}_{max}$ [kPa]		Variation of peak $\overline{\sigma_{T}}_{max}$ when ΔE increases from $0\ W/m$ to $210\ W/m$ [%]
		Proposed method using $\Delta E = 0\ W/m$	Proposed method using $\Delta E = 210\ W/m$	
600	1U	1160.3	887.4	−23.5
	2U	1510.1	1342.5	−11.1
	3U	1682.5	1559.9	−7.3
900	1U	597.5	462.1	−22.7
	2U	806.6	722.1	−10.5
	3U	918.6	855.6	−6.9

Table 5 Magnitudes of peak $\overline{\sigma_{T}}_{max}$ given by the proposed method using $\Delta E = 0\ W/m$ and $210\ W/m$ and the percentage reduction of peak $\overline{\sigma_{T}}_{max}$ when ΔE increases from $0\ W/m$ to $210\ W/m$

It can be observed from Figure 20 and Table 5 that relatively limited changes in the predicted evolution of axial stresses acting on the pile were determined, particularly when compared to the very large range considered in this study of possible temperature profiles within the heat exchanger pipes (represented in the proposed method by $T_{in,mid}$ and $T_{out,mid}$), herein determined based on an assumed thermal performance (ΔE). Moreover, the obtained results suggest that the sensitivity of the proposed method to ΔE, while practically independent of the pile diameter, varies significantly with pipe arrangement. As the number of U-loops increase, for instance, from one to three, ΔE per U-loop reduces from $210\ W/m$ to $70\ W/m$. As a result, the estimated drop in temperature between the inlets and outlets is smaller when a larger number of U-loops is used and becomes more similar to the case when $\Delta E = 0\ W/m$ is assumed. This explains the smaller difference in axial stresses obtained for the two extreme cases considered when the number of U-loops increase. As expected, the maximum thermally-induced axial stresses are determined for $\Delta E = 0\ W/m$, suggesting that this value can be used when either a conservative design is required or when considerable uncertainty surrounds the assumed temperature profiles along the heat exchanger pipes.

4 CONCLUSIONS

In the first part of this paper, the response of thermo-active piles is investigated by performing detailed coupled three-dimensional (3D) thermo-hydro-mechanical (THM) finite element (FE) analyses on $600mm$ and $900mm$ diameter piles with different pipe arrangements (1U, 2U and 3U), where thermal loading is applied by simulating explicitly the circulation of hot water through heat exchanger pipes. The results of these analyses highlighted a number of interesting aspects of the behaviour of these geostructures, which are summarised as follows.

a) As the pile is heated up, non-uniform distributions of temperature, and hence axial stresses, develop within the cross-section.
b) When the number of U-loops increases, a higher average and more uniformly distributed temperature is obtained in the cross-section, leading to considerably larger peak thermally-induced axial stresses.
c) Stresses are larger in the $600mm$ pile than in the $900mm$ pile for the same pipe arrangement, due to higher average temperatures being reached in the former, where each U-loop is required to heat up a smaller volume of concrete.
d) Peak values of axial stress obtained from the 3D analyses amount to about 20%-50% of the axial stress at an equivalent depth resulting from static loading, further demonstrating the relative importance of thermal loading.
e) The obtained thermally-induced axial stresses are shown to be significantly larger than those recommended by current design charts (GSHPA, 2012), although such differences reduce considerably with time, highlighting the importance of modelling accurately the transient response of thermo-active structures.

However, while these analyses provide valuable insight into the behaviour of these thermo-active structures, they require significant computational resources, which may render them impractical for routine engineering design. As a result, a simplified method to predict thermally-induced axial stresses is proposed in the second part of this paper. According to the devised method, stresses are estimated by carrying out a simpler axisymmetric analysis where the modelling of heat exchanger pipes is replaced by the use of a prescribed temperature boundary condition. The applied temperature is obtained directly from a 2D thermal analysis which models explicitly the disposition of the heat exchanger pipes within the cross-section of the pile. It is suggested that the power of the thermo-active pile estimated based on its characteristics can be used to determine the boundary conditions to be used in this analysis. In this paper, it is found that an assumption of $35\ W$ per m^2 of earth-contact area, as suggested by Brandl (2006) for piles of diameter $\geq 600mm$, yields accurate and slightly conservative predictions of peak stresses in both $600mm$ and $900mm$ piles. However, in scenarios where the anticipated thermal performance is uncertain, the proposed method is shown to be consistently conservative when the design inlet temperature is prescribed at all the heat sources included in the 2D plan analysis. Lastly, while the proposed simplified method has been established for a stratigraphy featuring a single material, it is expected that similar high levels of performance are obtained for layered deposits. In effect, the only aspect of the proposed methodology where soil layering is not explicitly considered is the 2D thermal analysis used to establish the boundary conditions to be applied in the axisymmetric THM analysis. Therefore, in soil deposits characterised by sharp contrasts in the thermal conductivity values of different layers, either a weighted average of this quantity can be used in the 2D thermal analysis or multiple sections along the pile length can be considered. Further research to clarify the impact of this additional simplification is required.

ACKNOWLEDGEMENTS

The first author is funded by the Imperial College President's PhD Scholarship and the Engineering and Physical Sciences Research Council (EPSRC) (grant number: EP/R512540/1) and the second author wishes to acknowledge the support from the Department of Civil and Environmental Engineering of Imperial College London through a Skempton Scholarship.

REFERENCES

Amatya, B. L., Soga, K., Bourne-Webb, P. J., Amis, T. & Laloui, L. (2012) Thermo-Mechanical Behaviour of Energy Piles. *Géotechnique*, **62** (6), 503-519.

Anongphouth, A., Maghoul, P. & Alfaro, M. (2018) Numerical Modeling of Concrete Energy Piles Using a Coupled Thermo-Hydro-Mechanical Model. In: *71st Canadian Geotechnical Conference, Edmonton, Alberta, Canada*.

Batini, N., Rotta Loria, A. F., Conti, P., Testi, D., Grassi, W. & Laloui, L. (2015) Energy and Geotechnical Behaviour of Energy Piles for Different Design Solutions. *Applied Thermal Engineering*, **86**, 199-213.

Bodas Freitas, T. M., Cruz Silva, F. & Bourne-Webb, P. J. (2013) The Response of Enery Foundations under Thermo-Mechanical Loading. *Proceedings of the 18th International Conference on Soil Mechanics and Geotechnical Engineering, Paris, France*. pp. 3347-3350.

Bourne-Webb, P. J., Amatya, B., Soga, K., Amis, T., Davidson, C. & Payne, P. (2009) Energy Pile Test at Lambeth College, London: Geotechnical and Thermodynamic Aspects of Pile Response to Heat Cycles. *Géotechnique*, **59** (3), 237-248.

Bourne-Webb, P. J., Amatya, B. & Soga, K. (2013) A Framework for Understanding Energy Pile Behaviour. *Proceedings of the Institution of Civil Engineers - Geotechnical Engineering*, **166** (2), 170-177.

Bourne-Webb, P. (2013) Observed Response of Energy Geostructures. *Energy geostructures: Innovation in underground engineering*, 45-77.

Brandl, H. (2006) Energy Foundations and Other Thermo-Active Ground Structures. *Geotechnique*, **56** (2), 81-122.

Cui, W., Gawecka, K. A., Potts, D. M., Taborda, D. M. G. & Zdravković, L. (2016) Numerical Analysis of Coupled Thermo-Hydraulic Problems in Geotechnical Engineering. *Geomechanics for Energy and the Environment*, **6**, 22-34.

Cui, W., Gawecka, K. A., Potts, D. M., Taborda, D. M. G. & Zdravković, L. (2018a) A Petrov-Galerkin Finite Element Method for 2d Transient and Steady State Highly Advective Flows in Porous Media. *Computers and Geotechnics*, **100**, 158-173.

Cui, W., Potts, D. M., Zdravkovic, L., Gawecka, K. A. & Taborda, D. M. G. (2018b) An Alternative Coupled Thermo-Hydro-Mechanical Finite Element Formulation for Fully Saturated Soils. *Computers and Geotechnics*, **94**, 22-30.

Faizal, M., Bouazza, A. & Singh, R. M. (2016) Heat Transfer Enhancement of Geothermal Energy Piles. *Renewable and Sustainable Energy Reviews*, **57**, 16-33.

Gawecka, K. A., Potts, D. M., Taborda, D. M. G., Cui, W. & Zdravkovic, L. (2016) Effects of Transient Phenomena on the Behaviour of Thermo-Active Piles. *Proceedings of the 1st International Conference on Energy Geotechnics, ICEGT 2016*. pp. 71-78.

Gawecka, K. A., Taborda, D. M. G., Potts, D. M., Cui, W., Zdravković, L. & Haji Kasri, M. S. (2017) Numerical Modelling of Thermo-Active Piles in London Clay. *Proceedings of the Institution of Civil Engineers - Geotechnical Engineering*, **170** (3), 201-219.

Gawecka, K. A., Potts, D. M., Cui, W., Taborda, D. M. G. & Zdravković, L. (2018) A Coupled Thermo-Hydro-Mechanical Finite Element Formulation of One-Dimensional Beam Elements for Three-Dimensional Analysis. *Computers and Geotechnics*, **104**, 29-41.

Gawecka, K. A., Taborda, D. M. G., Potts, D. M., Sailer, E., Cui, W. & Zdravković, L. (2020) Finite-Element Modeling of Heat Transfer in Ground Source Energy Systems with Heat Exchanger Pipes. *International Journal of Geomechanics*, **20** (5).

GSHPA (2012) *Thermal Pile Design, Installation and Materials Standards*. Ground Source Heat Pump Association.

Hassani Nezhad Gashti, E., Malaska, M. & Kujala, K. (2014) Evaluation of Thermo-Mechanical Behaviour of Composite Energy Piles During Heating/Cooling Operations. *Engineering Structures*, **75**, 363-373.

Laloui, L., Nuth, M. & Vulliet, L. (2006) Experimental and Numerical Investigations of the Behaviour of a Heat Exchanger Pile. *International Journal for Numerical and Analytical Methods in Geomechanics*, **30** (8), 763-781.

Liu, R. Y. W. (2017) *Computational Study on Factors Influencing the Design of Thermo-Active Piles*. MEng dissertation. Imperial College London, London.

Liu, R. Y. W., Taborda, D. M. G., Gawecka, K. A., Cui, W. & Potts, D. M. (2019) Computational Study on the Effects of Boundary Conditions on the Modelled Thermally Induced Axial Stresses in Thermo-Active Piles. *Proceedings of the XVII European Conference on Soil Mechanics and Geotechnical Engineering, Reykjavik, Iceland*.

Loveridge, F., Powrie, W. & Nicholson, D. (2014) Comparison of Two Different Models for Pile Thermal Response Test Interpretation. *Acta Geotechnica*, **9** (3), 367-384.

Measham, P., Taborda, D., Zdravkovic, L. & Potts, D. (2014) Numerical Simulation of a Deep Excavation in London Clay. *Proceedings of the Proceedings of the 8th European Conference on Numerical Methods in Geotechnical Engineering, Delft, The Netherlands*. Taylor & Francis, London, UK, pp. 771-776.

Merton Council (2010) *Sustainable Design and Construction Evidence Base: Climate Change in the Planning System*. Merton Council.

Olgun, C. G., Ozudogru, T. Y., Abdelaziz, S. L. & Senol, A. (2014) Long-Term Performance of Heat Exchanger Piles. *Acta Geotechnica*, **10** (5), 553-569.

Potts, D. M. & Zdravkovic, L. (1999) *Finite Element Analysis in Geotechnical Engineering: Theory*. London, Thomas Telford Publishing.

Potts, D. M. & Zdravkovic, L. (2001) *Finite Element Analysis in Geotechnical Engineering: Application.* London, Thomas Telford Publishing.

Rotta Loria, A. F. & Laloui, L. (2016) Analysis of Thermally Induced Mechanical Interactions in Energy Pile Groups. In: Wuttke, F., Bauer, S. and Sanchez, M. (eds.) *1st International Conference on Energy Geotechnics, ICEGT 2016, Kiel, Germany*. pp. 171-178.

Sailer, E., Taborda, D. M. G., Zdravković, L. & Potts, D. M. (2019) Fundamentals of the Coupled Thermo-Hydro-Mechanical Behaviour of Thermo-Active Retaining Walls. *Computers and Geotechnics*, **109**, 189-203.

Taborda, D. M. G., Potts, D. M. & Zdravković, L. (2016) On the Assessment of Energy Dissipated through Hysteresis in Finite Element Analysis. *Computers and Geotechnics*, **71**, 180-194.

World Wide Fund For Nature (2019) Climate Mitigation by Merton Rule, Available from: https://wwf.panda.org/?204444/Merton-London-climate-rule [Accessed: 20th February 2020]

Yavari, N., Tang, A. M., Pereira, J. M. & Hassen, G. (2014) A Simple Method for Numerical Modelling of Mechanical Behaviour of an Energy Pile. *Géotechnique Letters*, **4** (2), 119-124.

APPENDIX A

In the Imperial College Generalised Small-Strain Stiffness (IC.G3S) model (Measham et al., 2014; Taborda et al., 2016), the degradation of tangent shear modulus G_{tan} with deviatoric strain E_d is given by Equation A1 and the degradation of tangent bulk modulus K_{tan} with volumetric strain ε_{vol} is given by Equation A3.

$$G_{tan} = G_{ref}\left(\frac{p'}{p'_{ref}}\right)^{m_G}\left[R_{G,min} + \frac{1 - R_{G,min}}{1 + \left(\frac{E_d}{a}\right)^{b}}\right] \tag{A1}$$

where

$$E_d = \frac{2}{\sqrt{6}}\sqrt{(\varepsilon_1 - \varepsilon_2)^2 + (\varepsilon_2 - \varepsilon_3)^2 + (\varepsilon_1 - \varepsilon_3)^2} \tag{A2}$$

$$K_{tan} = K_{ref}\left(\frac{p'}{p'_{ref}}\right)^{m_K}\left[R_{K,min} + \frac{1 - R_{K,min}}{1 + \left(\frac{|\varepsilon_{vol}|}{r}\right)^{s}}\right] \tag{A3}$$

where

$$\varepsilon_{vol} = \varepsilon_1 + \varepsilon_2 + \varepsilon_3 \tag{A4}$$

APPENDIX B

Figures B1 to B3 show the distribution of temperature and thermally induced axial stresses within the $600mm$ pile cross-section for 1U, 2U and 3U pipe arrangements, respectively, while Figure B4 shows the distribution of $\overline{\sigma_T}$ along the pile length, at the time instants when the corresponding values of $\overline{\sigma_T}_{max}$ are the largest over the 5 months of heating for the $600mm$ pile.

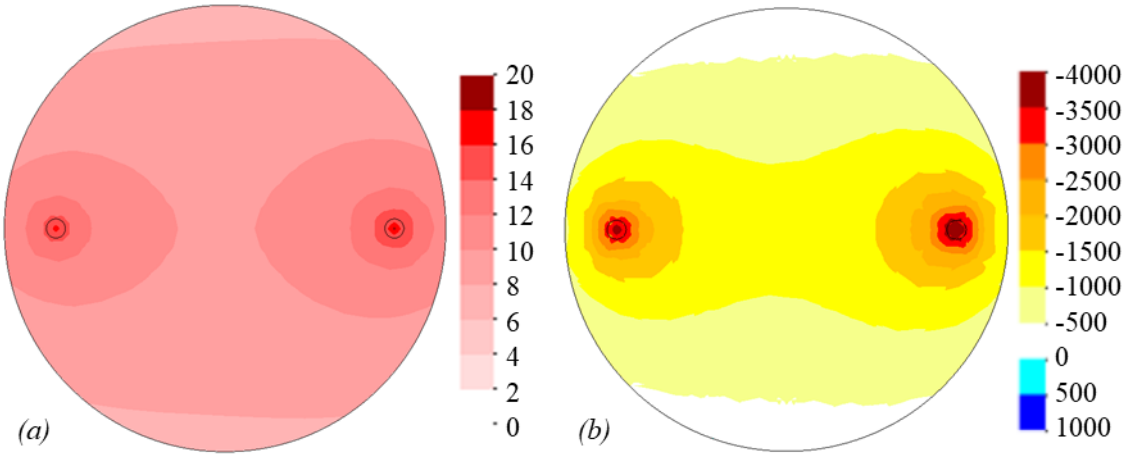

Figure B1 Distribution of (a) temperature change $[°C]$ and (b) thermally-induced axial stresses σ_T $[kPa]$ within the cross-section of the $600mm$ pile with 1U pipe arrangement at $t = 7\ days$ and $17m$ depth

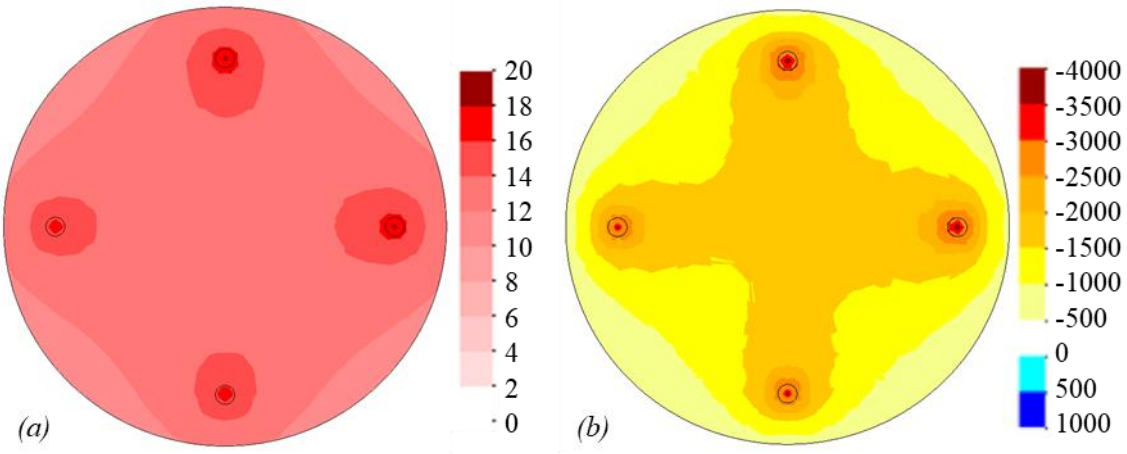

Figure B2 Distribution of (a) temperature change $[°C]$ and (b) thermally-induced axial stresses σ_T $[kPa]$ within the cross-section of the $600mm$ pile with 2U pipe arrangement at $t = 4\ days$ and $17m$ depth

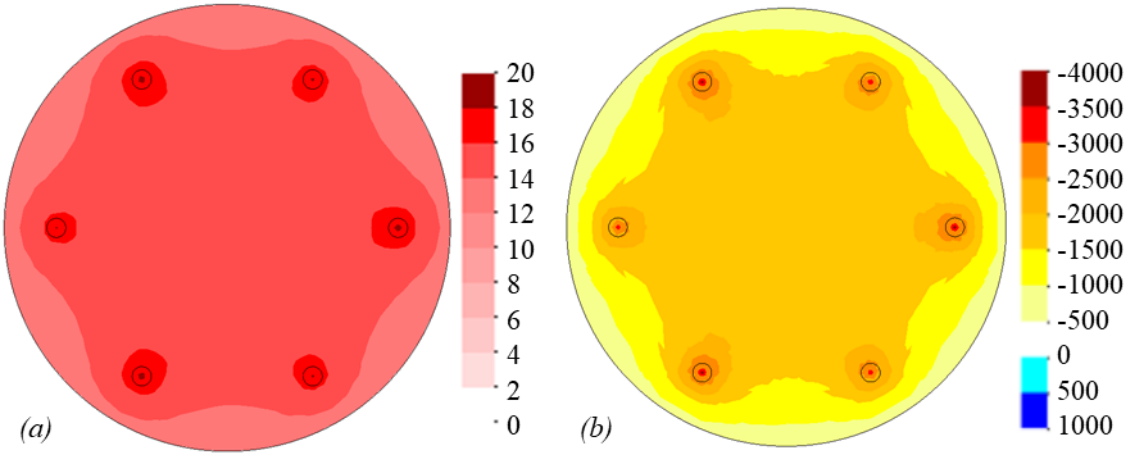

Figure B3 Distribution of (a) temperature change $[°C]$ and (b) thermally-induced axial stresses σ_T $[kPa]$ within the cross-section of the $600mm$ pile with 3U pipe arrangement at $t = 2.5\ days$ and $17m$ depth

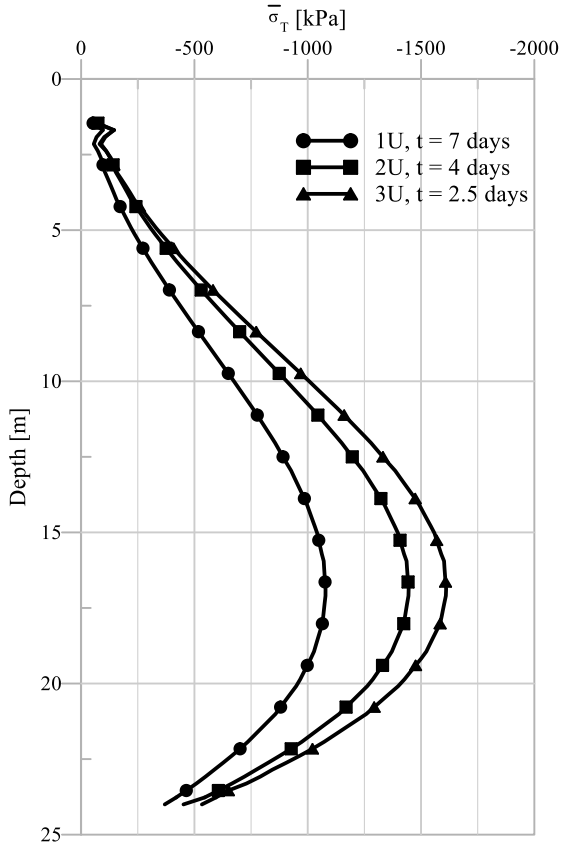

Figure B4 Distribution of $\overline{\sigma_T}$ along the pile length for the analyses on the $600mm$ pile

APPENDIX C

Figure C1 shows for the $600mm$ diameter pile and $900mm$ diameter pile the evolutions of $\overline{\sigma_T}_{max}$ with time obtained in the 3D analyses compared with those obtained from axisymmetric analyses performed assuming a uniform temperature change of 20^oC (equal to that applied at the pipe inlet in the 3D analyses) across the piles. In scenario I, the temperature change occurs instantaneously, while in scenario II it takes place over 1 month, after which point the temperature remains constant.

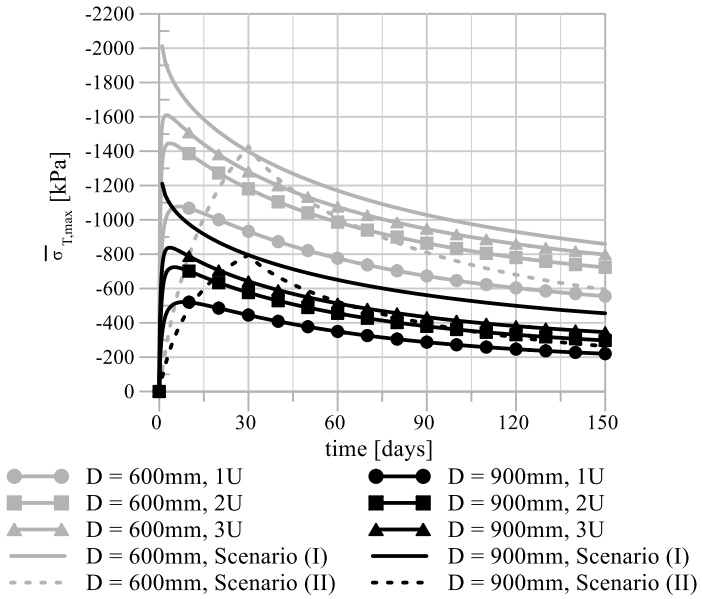

Figure C1 Evolutions of $\overline{\sigma_T}_{max}$ with time obtained from the 3D analyses and the axisymmetric analyses where the pile is heated by a uniform change in temperature of 20^oC for both the $600mm$ and $900mm$ piles